Ag-Functionalized CuWO4/WO3 nanocomposites for solar water splitting

Salimi, Reza; Sabbagh Alvani, A. A.; Mei, Bastian Timo; Naseri, N.; Du, Shangfeng; Mul , Guido

DOI:
10.1039/C8NJ05625K

Document Version
Peer reviewed version

Citation for published version (Harvard):
Salimi, R, Sabbagh Alvani, AA, Mei, BT, Naseri, N, Du, S & Mul , G 2019, 'Ag-Functionalized $CuWO_4/WO_3$ nanocomposites for solar water splitting', *New Journal of Chemistry*, vol. 43, no. 5, pp. 2196-2203. https://doi.org/10.1039/C8NJ05625K

Journal

ARTICLE

Ag-Functionalized $CuWO_4/WO_3$ Nanocomposite for Solar Water Splitting

Received 00th January 20xx,
Accepted 00th January 20xx

DOI: 10.1039/x0xx00000x

www.rsc.org/

R. Salimi [a,b,c], A.A. Sabbagh Alvani [*,a,b], B.T. Mei[c], N. Naseri [d,e], S.F. Du[f], G. Mul[c]

Ag-functionalized $CuWO_4/WO_3$ heterostructures were successfully prepared via a polyvinyl pyrrolidone (PVP)-assisted sol-gel (PSG) route. Thin films prepared by electrophoretic deposition were used as photoanodes for photoelectrochemical (PEC) water splitting. Compared to pristine $CuWO_4$ and WO_3 films, a significant enhancement of the photocurrent (3-4 times) at the thermodynamic potential for oxygen evolution (0.62 V vs. Ag/AgCl) was obtained for Ag-functionalized $CuWO_4/WO_3$ photoanodes. The obtained enhancement is shown to be derived from a synergic contribution of heterostructure formation ($CuWO_4/WO_3$) and improvements of light utilization by Ag-induced surface plasmon resonance (SPR) effects. Accordingly, a photocurrent of 0.205 mA/cm^2 at 0.62 V vs. Ag/AgCl in neutral conditions (without hole scavengers) under front-side simulated AM1.5G illumination was achieved. A detailed analysis of the obtained PEC data alongside with performed impedance measurements suggests that charge seperation is significantly improved for the prepared Ag-functionalized $CuWO_4/WO_3$ photoanodes. Our work offers beneficial insights to design new plasmonic metal/heterostructured nanocomposites for energy conversion applications.

1. Introduction

Harvesting solar energy and storing surplus "green" electricity in chemical bonds (so-called green fuels) is considered necessary to allow for the replacement of fossil fuels and to mitigate increasing environmental concerns [1, 2]. Production of hydrogen by, among others, photo-electrochemical (PEC) water decomposition has been frequently suggested as promising technology.

The development of inexpensive and environmentally benign materials that can harvest significant fractions of solar irradiation, efficiently create and separate charge carriers, and allow for electrochemical water reduction or oxidation, is one of the main challenges of ongoing research [3-8]. Semiconducting metal oxides such as TiO_2 and Fe_2O_3 have been primarily used as photoanode materials. Low cost and high chemical stability are advantageous, but large band gaps, insufficient charge-carrier mobility, small diffusion lengths, and unfavourable kinetics for water oxidation, preclude their usage [9-12]. More recently, $CuWO_4$ was shown to be a promising candidate for PEC applications [13-17]. Its band gap (about 2.2-2.4 eV) closely resembles the optimal value for water splitting in tandem devices [13-15], and theoretically solar to hydrogen (STH) efficiencies of up to 13% are achievable [15, 18]. Unfortunately, a relatively low absorption coefficient and a high bulk charge transfer resistance (due to the empty orbital of Cu

[a.] Color & Polymer Research Center, Amirkabir University of Technology (Tehran Polytechnic), P.O. Box 15875-4413, Tehran, Iran
[b.] Department of Polymer Engineering and Color Technology, Amirkabir University of Technology, (Tehran Polytechnic), P.O. Box 15875-4413, Tehran, Iran
[c.] Photocatalytic Synthesis Group, Faculty of Science and Technology, MESA+ Institute for Nanotechnology, University of Twente, Enschede, The Netherlands
[d.] Department of Physics, Sharif University of Technology, Tehran, Iran
[e.] Condensed Matter National Laboratory, Institute for Research in Fundamental Sciences, Tehran, Iran
[f.] School of Chemical Engineering, University of Birmingham, Birmingham, UK
E-mail: Sabbagh_alvani@aut.ac.ir

($3dx^2$-y^2)) negatively affect the overall water splitting efficiency [13-15, 18]. Generally, for tungstate-based semiconductors, various strategies have been reported to improve their usability [19-29]. Especially fabrication of heterostructured systems, and functionalizing semiconductor surfaces with metallic (plasmonic) nanoparticles have been widely used [18, 30-35]. Dass et al. [36] successfully incorporated plasmonic metal nanoparticles into heterostructured $BiVO_4/Fe_2O_3$ and Slabon et al [37] fabricated $CuWO_4$-based heterojunctions ($CuWO_4/Ag_2NCN$). Thus, it is evident that formation of n-n heterojunction configurations results in favourable properties for photo-electrochemical (PEC) applications by facilitating interfacial charge transfer, and retarding recombination of charge carriers [14]. Photon absorption and charge generation/separation might generally be affected by surface plasmon resonance (SPR) phenomena [38]. Similarly, we recently reported on the significant increase in photocatalytic activity of $CuWO_4/WO_3$ composites by modification with Ag nanostructures for water treatment applications [39].

Due to the beneficial properties of the composites, in this work, Ag-decorated $CuWO_4/WO_3$ heterostructures were prepared via the PVP-assisted sol-gel (PSG) synthesis. In-situ decoration was achieved by $AgNO_3$ addition during the synthesis allowing for the preparation of well-dispersed Ag NPs, causing a good interaction with $CuWO_4/WO_3$ heterostructures. Here, specifically the influence of the individual modifications (heterojunction and plasmon resonance) on the photoelectrochemical (PEC) characteristics of electrodeposited thin film samples were evaluated, and it will be shown that for Ag-modified $CuWO_4/WO_3$ composites, improved charge separation efficiencies result in significant improvements in PEC performance.

2. Experimental Procedure

2.1. Materials Synthesis and Film Preparation

Copper nitrate hydrate, polyvinylpyrrolidone (PVP, M_w = 29000), ammonium metatungstate hydrate (AMT), $AgNO_3$ and ethylene glycol (EG), all with high purity grade (99%, Sigma-Aldrich) were used. $CuWO_4/WO_3$ was prepared similar to our previous report [39]. In short, a PVP-assisted sol-gel (PSG) approach was used (Scheme S1) in which, 0.242 g of $Cu(NO_3)_2.3H_2O$ dissolved in 15 mL ethylene glycol were mixed with solution of 0.296 g AMT dissolved in 1 mL of distilled water and PVP. The obtained solution was heated to 95°C in an oil bath until a viscous green suspension was obtained (approx. 6 h). For in-situ Ag decoration of the composite, 1 ml of silver nitrate solution (0.05M in EG) was slowly added within 1 hour to the hot suspension under stirring. After aging and drying at 120°C, the obtained powder was calcined at 525°C for 90 min. Thin film photoanodes were prepared by electrophoretic deposition on FTO glass (see Figure S1 and SI for further information) [40].

2.2. Materials Characterization

Photoluminescence (PL) (Perkin-ElmerLS-55), Raman spectroscopy (Bruker, Senerra), X-ray diffraction (XRD, Inel, EQuniox 3000, with Cu Kα radiation, lambda = 0.154 nm), UV-Vis spectrophotometry (Perkin Elmer Lambda 40), scanning electron microscopy (SEM/EDX, Seron Technologies AIS2100) and N_2 physi-sorption (Micromeritics ASAP 2010) were used to analyse the samples.

2.3. Photoelectrochemical (PEC) Characterization

PEC measurements were performed in a three-electrode configuration (VersaSTAT 4 potentiostat) using the obtained thin film samples as working electrode (exposed area of 0.28 cm^2). A Pt wire and an Ag/AgCl (saturated KCl) electrode were used as counter and reference electrode, respectively. 0.1 M phosphate buffer (pH 7) with and without hole scavengers (0.1 M H_2O_2 and Na_2SO_4) was used as electrolyte. Illumination (100 mW/cm^2 AM1.5G) was achieved with a Newport light source. The light response was probed by chopped light linear sweep voltammetry (LSV), and cyclic voltammetry (CV) and chronoamperometry (I-t) was used to evaluate the photoanode stability (at 0.6 V vs. Ag/AgCl). Electrochemical impedance spectroscopy (EIS) and Mott-Schottky analysis of the as-prepared thin film samples were conducted using a commercially available three-electrode Autolab system (PGSTAT302N). Impedance measurements were performed at an amplitude of 10 mV over a frequency range of 0.1 Hz to 100 kHz in Na_2SO_4 (0.1 M).

3. Results and Discussion

3.1. Materials Characterization

Both phases of WO_3 (JCPDS data card No. 43-1035) and $CuWO_4$ (JCPDS data card No. 72-0616) were revealed by X-ray diffraction

(Fig. 1), as already previously shown [39]. Moreover, the average primary crystallite sizes of $CuWO_4/WO_3$ were estimated to be 28-31 nm, using the Scherrer formula [39, 41, 42].

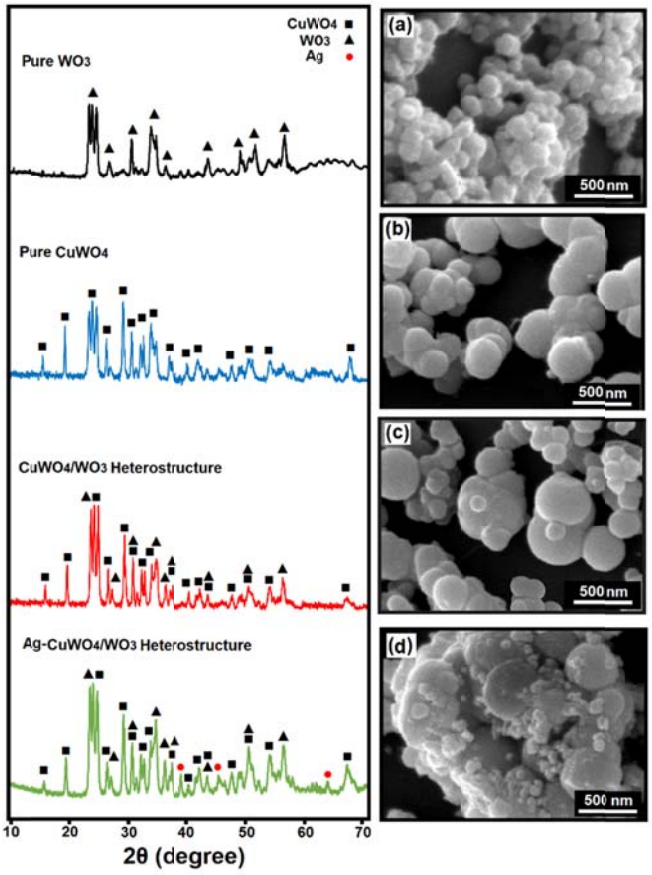

Figure 1. XRD patterns (left) and SEM images (right) of the as-prepared samples (The XRD pattern of the pure composite (red curve) derived from our previous publication for better comparison [39])

The materials were further examined by SEM (Fig. 1). Uniform spherical particles of $CuWO_4/WO_3$ with sizes in the range of 100 - 500 nm were obtained by the PVP-assisted method governed by the chelating properties of PVP, preventing massive agglomeration during the calcining process [39, 43, 44]. Likewise the synthesis resulted in high surface area materials (about 54.8 m^2g^{-1}, consistent with the performed BET analysis, Fig. S2).

In addition to the diffraction lines of the pristine composite, diffraction peaks at 38.8°, 45.1° and 64.5° are indicative of the (111), (200) and (220) planes of face-centred cubic (FCC) silver (JCPDS card no. 04-0783). This affirms the successful in-situ modification of $CuWO_4/WO_3$ with silver nanoparticles (NPs).

The morphology of the Ag surface modified $CuWO_4/WO_3$ composite is depicted in Fig. 1d. Ag nanoparticles (primary particle size 19-21 nm estimated from XRD) are observed with appropriate dispersion on the surface of the composite particles.

Based on a probable reaction happening during the employed in-situ sol-gel synthesis, Ag^+ ions are reduced by EG and Ag nanoparticles nucleate via a homogeneous process on active growth sites of the $CuWO_4/WO_3$ composite. In principle, the surface energies are favourable for large particles and small Ag nanoparticles are disposed to grow via Ostwald ripening. Again, the presence of PVP during the synthesis is important to achieve well dispersed Ag nanoparticles and allows for kinetically controlled growth of crystal faces of Ag nanocrystals [45].

Thus, similar to the $CuWO_4/WO_3$ composites, Ag-functionalized $CuWO_4/WO_3$ nanocomposites were prepared with high crystallinity. Semiconductors with high crystallinity are expected to possess lower (bulk) defect densities, and severe recombination of photo-generated charge carriers might therefore be less likely for the synthesised materials.

The Raman spectrum of the PSG-prepared Ag functionalized product also displays main fingerprint vibration bands of both phases (Fig. 2a) with some protuberant peaks [39, 46, 47]. The signals assigned to Ag nanocrystals cannot be identified in the Raman spectra.

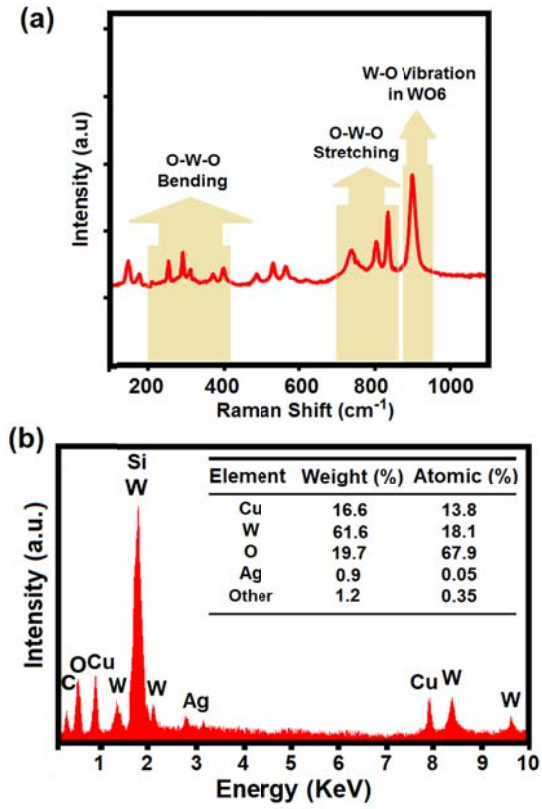

Figure 2. (a) Raman spectrum and (b) EDX analysis of the PSG-prepared Ag-functionalized composite

Figure 3. (a) UV-Vis spectra and (b) PL spectra (λ_{ex} = 340 nm) of the as-synthesized powder samples (data related to WO_3 and unmodified $CuWO_4/WO_3$ samples derived from our recent publication for better comparison [39]).

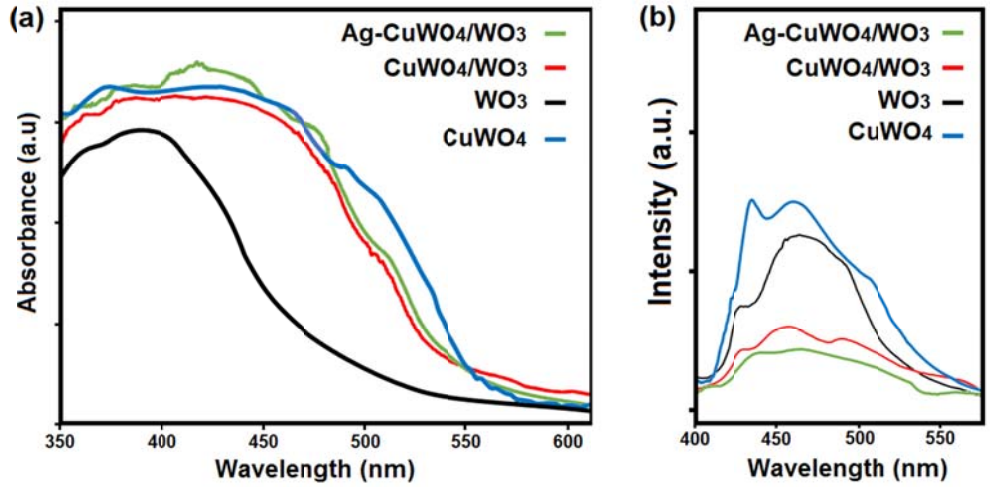

Along with the SEM measurements, EDX (Fig. 2b) analysis was performed, confirming the presence of Cu, W and Ag in the sample. The determined content of the individual components is in good agreement with the intended loading. In conclusion, the successful synthesis of Ag-functionalized $CuWO_4/WO_3$ via PSG method was confirmed.

UV-Vis spectra of the PSG-synthesized pure and Ag-loaded $CuWO_4/WO_3$ heterostructures (illustrated in Fig. 3a) disclose two overlapping charge transfer transitions in the visible region, as expected for $CuWO_4$ [39, 48]. Moreover, the hybridization of the Cu^{2+} 3d-orbitals with the O (2p) states results in the lower band gap of the PSG-derived $CuWO_4/WO_3$ and the Ag-functionalized $CuWO_4/WO_3$ heterostructures (estimated about 2.28-2.33 eV), compared to pure WO_3 [14, 39, 48]. Additionally, for Ag-functionalized $CuWO_4/WO_3$, a slight increase in absorbance, especially at approximately 420-480 nm, is in good agreement with

various reports for localized surface plasmon resonances (LSPR) induced by decorated Ag nanoparticles [35, 49, 50].

Charge trapping and recombination of photo-generated electron/hole pairs in the electrodeposited thin films were assessed by photoluminescence (PL) analysis, measured using a 340 nm laser for excitation (Fig. 3b). The radiative emission intensity of the Ag decorated heterostructures are evidently reduced.

The observed quenching is tentatively assigned to an effective suppression of electron-hole recombination pathways due to the SPR effects of Ag NPs. As previously reported, the charge transfer between $CuWO_4$ and WO_3 interface with staggered band configuration, causing a local built-in potential, facilitates separation of charge carriers in the $CuWO_4/WO_3$ heterostructures [39].

3.2. Photoelectrochemical (PEC) Studies

Typical linear sweep voltammetry (LSV) scans obtained in potassium phosphate buffer solution (pH7) for front-side illuminated samples are presented in Fig. 4. Independent on the exact composition of the electrode, for all samples a positive response to light-stimuli was observed as evidenced by the generated anodic photocurrents. For pristine WO_3 and $CuWO_4$ films, a photocurrent density of approximately 0.048 and 0.075 mA/cm^2 at 0.62 V vs Ag/AgCl (thermodynamic redox potential for water oxidation) were measured. For the two composite electrodes, significant improvements were obtained. Compared to pure $CuWO_4$, photocurrent densities of 0.152 mA/cm^2 (2 times enhancement) and 0.205 mA/cm^2 (2.7 times enhancement) were measured for $CuWO_4/WO_3$ and Ag-functionalized $CuWO_4/WO_3$ composites, respectively. Thus, compared with other recent reports for similar tungstate-based structures, promising photocurrents were achieved [21, 24, 31, 51, 52].

Figure 4. The photoelectrochemical response characterized by linear sweep voltammetry (LSV) without hole scavenger (black) and with hole scavenger (red)

Moreover, PEC experiments in the presence of hole scavengers were also performed (with 0.1 M H_2O_2 and Na_2SO_4) for rapid consumption of photo-generated holes at the semiconductor-electrolyte interface (η_{cat}~1). As expected, for all samples the measured photocurrent densities are significantly increased. For instance, the photocurrent increased to 0.365 mA/cm^2 (at 0.62 V) for Ag-functionalized composites.

The light absorption, electron/hole pair separation and catalytic efficiency of the electrodeposited thin films were assessed using the previously reported analysis by Dotan et al [53] to better identify the controlling factors in PEC performance. The generated photocurrent density in aqueous electrolytes is calculated by:

$$J_{H2O} = J_{abs} \times \eta_{sep} \times \eta_{cat} \quad (1)$$

where J_{H2O} is the measured photocurrent density, η_{cat} is the efficiency of interfacial charge injection and η_{sep} is the photo-generated charge separation efficiency. For the absorption current

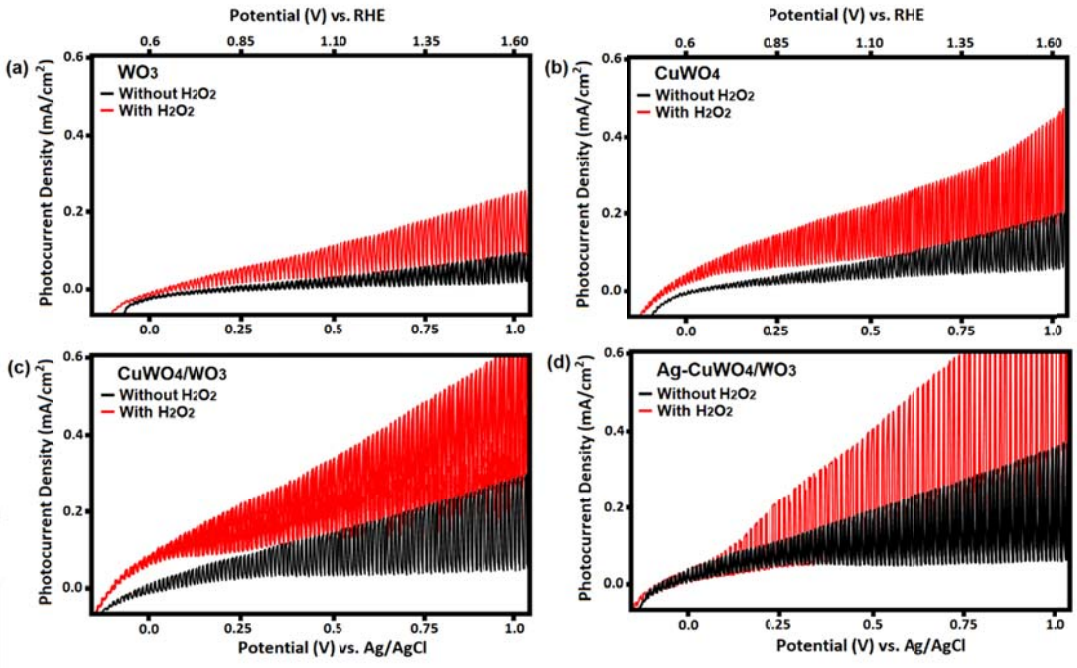

density, J_{abs}, it is assumed that all generated charge carrier pairs take part in the water splitting reaction by considering 100% faradaic and catalytic efficiency. J_{abs} is estimated as [51, 54]:

$$J_{abs} = e \int_{350}^{600} \Phi_{\lambda} (A)\, d\lambda \quad (2)$$

where e is the electron charge, Φ_{λ} is the photon flux in $m^2\ s^{-1}\ nm^{-1}$ and A is the portion of photons absorbed per incident ones on the sample (estimated by UV-Vis analysis). Accordingly, the absorption current density, J_{abs} was measured to be 2.96, 5.98, 5.45 and 5.86 mA/cm^2 for WO_3, $CuWO_4$, $CuWO_4/WO_3$ and Ag-functionalized $CuWO_4/WO_3$ composite films, respectively.

Using equation (1) and comparing PEC photocurrent densities obtained with (J_{H2O2}) or without the hole scavengers (J_{H2O}) (eq. 3), the catalytic efficiency (η_{cat}) can be calculated. Similarly, the charge separation efficiency (η_{sep}) of the electrodeposited films can be obtained by J_{abs} and J_{H2O2} following eq. 4:

$$\eta_{cat} = J_{H2O}/J_{H2O2} \quad (3)$$

$$\eta_{sep} = J_{H2O2}/J_{abs} \quad (4)$$

Fig. 5 a, b depicts the potential-dependent results, revealing that both η_{cat} and η_{sep} increase significantly upon composite fabrication and Ag-functionalization. Specifically, at the oxygen evolution potential, the separation efficiencies of only 3.5% and 2.6% for the pure WO_3 and $CuWO_4$ photoanodes were enhanced to 5.3% and 6.2% for the composite materials.

Figure 5. (a) Separation and (b) catalytic efficiencies of the as-prepared thin films

For the catalytic efficiencies, a tangible improvement from 45% for pure WO_3 to 56% for the Ag-functionalized composite photoanode was achieved.

The results of the performed analysis were strengthened by electrochemical impedance measurements and Mott-Schottky (MS) analysis. As indicated by the apparent semicircle in the Nyquist plots (Fig. 6), a decrease in charge transfer resistance across the electrode/electrolyte interface was observed in good agreement with the above presented data [39].

The capacitance measured at different potentials and a constant AC frequency (Mott-Schottky plot, Fig. S3) was analysed according to equation 5 [55]:

$$\frac{1}{C^2} = \frac{2}{N_D \varepsilon_0 \varepsilon e}\left[(E - E_{fb}) - \frac{K_B T}{e}\right] \quad (5)$$

where C is the space charge capacitance; ε_o is the permittivity of a vacuum, N_D is the electron carrier density; E is the applied bias; ε is the relative permittivity; K_B is the Boltzmann constant and T is the temperature. The positive slopes of the linear parts of the obtained curves (Fig. S3) confirm n-type characteristics for all samples. A substantial decrease of the slope in case of $CuWO_4/WO_3$ heterostructure indicates a significant increase of donor densities, thereby improving the charge mobility in the semiconductors. These trends clearly suggest that the composite fabrication and Ag-functionalization considerably facilitate the charge separation and interfacial charge transfer, thereby improving the PEC performance.

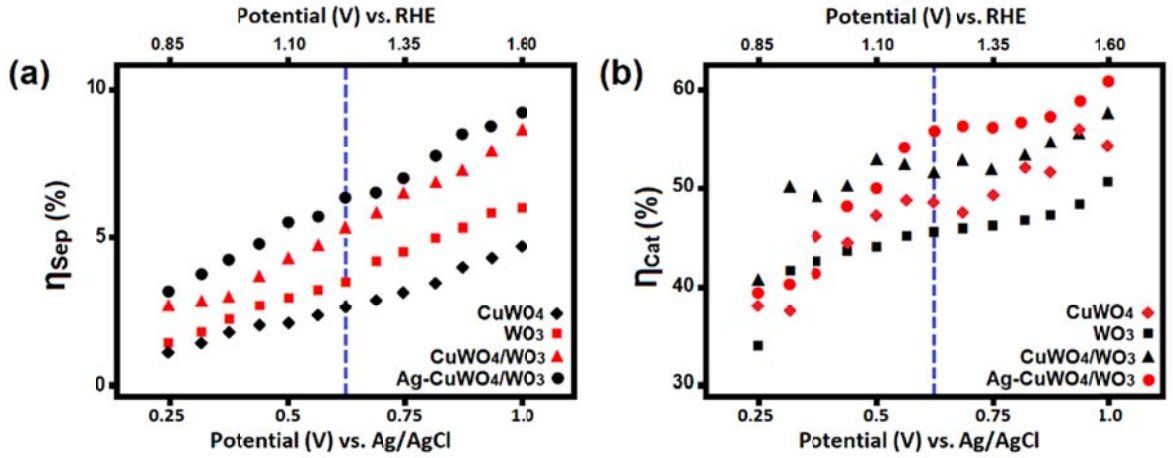

By extrapolation of the obtained Mott-Schottky data, flat band potentials (V_{fb}) were estimated for the different materials. For pure WO_3 and $CuWO_4$ films, flat band potentials of -0.015 and -0.075 V vs Ag/AgCl were obtained, in good agreement with recent literature [31, 56]. For $CuWO_4/WO_3$ heterojunctions, the flat band potential was estimated to be -0.045 V vs Ag/AgCl, indicative of an equilibrium formation and the renewal of a Fermi level.

Moreover, based on the obtained data and the calculation of band edges using the method of Ginley and Butler (for further information see SI) [39, 57, 58], an energy band structure diagram (Fig. 7a) was derived.

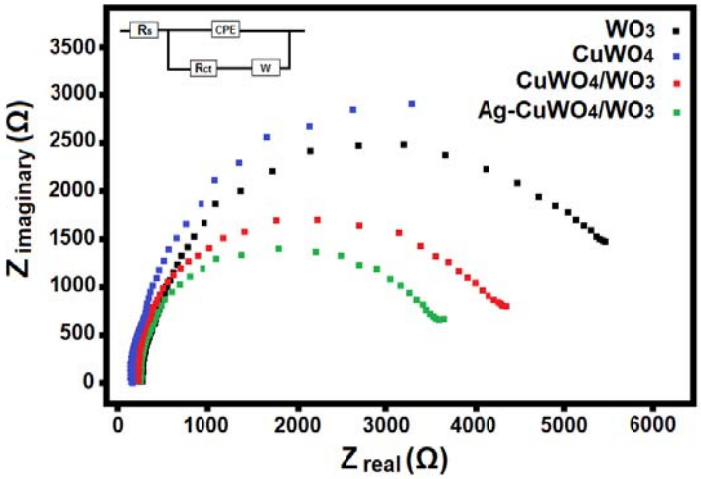

Figure 6. EIS Nyquist of the as-prepared thin films at the frequency range of 0.1 Hz to 100 KHz

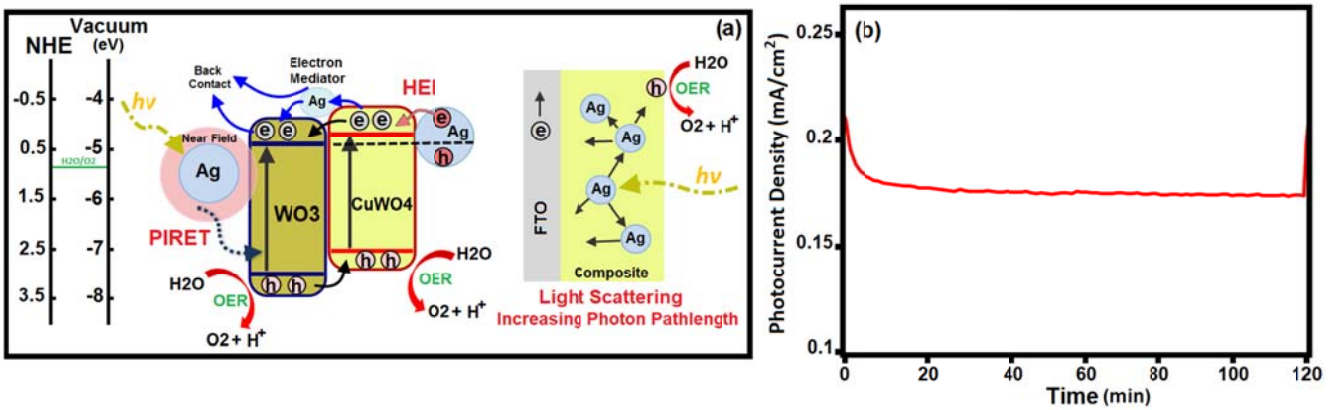

Figure 7. (a) Depiction of the energy diagram of $CuWO_4$ and WO_3 band positions, charge transfer/separation process and SPR effects (b) Chronoamperometry (at 0.62 V) of the Ag functionalized composite electrode in the electrolyte without hole scavengers

Clearly an offset between energy levels and the staggered type alignment of the junction reveals that $CuWO_4$ acts as a functional component injecting excited electrons to the CB of WO_3 and likewise extracting holes (from the VB of WO_3). These staggered band positions and redistribution of charge density allow for a built-in electric field which causes an effective charge separation, thereby reducing the recombination rate at the interface of the heterojunction [39, 59].

As indicated by the obtained PEC results, in-situ decoration of $CuWO_4/WO_3$ heterojunctions with Ag nanoparticles clearly allows for performance improvements. It is generally accepted that Ag NPs can enhance the photon absorption and charge carrier generation/separation of adjacent semiconductors [34, 38, 49, 60]. Various scenarios are possible and detangling the cause of the improvement is ongoing. Ag nanoparticles might affect the performance by 1) scattering of resonant photons (Fig. 7a, right) , 2) a plasmon-induced resonance energy transfer (PIRET) 3) a SPR-induced hot electron injection (HEI), as illustrated in figure 7a.

As already pointed out, UV-Vis measurements (Fig. 3a) show beneficial absorbance properties of the Ag-functionalized materials indicating that light scattering (due to different refractive index of NPs and bulk semiconductor, mainly by larger particles) rises the path length of photons which likely leads to a higher generation rate of excitons in the semiconductor. Moreover, due to the evident spectral overlap of the absorption region in $CuWO_4/WO_3$ and the SPR band of Ag NPs (420-480 nm), plasmon-induced resonance energy transfer (PIRET) by non-radiative strong dipole-dipole coupling with band edge states of semiconductors must be considered as another dominating effect for the improved absorption [38, 49, 60, 61].

The interaction of Ag nanoparticles and the semiconductor is also in agreement with the observed quenching of PL emission (Fig. 3b).

The localized electric fields around the plasmonic metal particles (PIRET) with the adjacent semiconductor allow for efficient separation of charge carriers on the surface of semiconductors (not bulk) and shorter diffusion of holes (or electrons) to the semiconductor surface [35, 49, 60]. Accordingly, a positive effect on the PEC performance is observed. Unlike the two SPR effects, hot electron injection effect (charge transfer) might be relatively weak due to the size of the obtained particles (> 20 nm) and generally short lifetimes of hot electrons. Finally, it should be pointed out that Ag nanocrystals could also act as electron acceptor, facilitating the electron transfer in-between particles and to the back contact. At the same time, the NPs located at the semiconductor/electrolyte interface might improve hole injection to the electrolyte due to the improved catalysis near the metal NPs [35, 36, 38, 49, 60]. Consequently, the observed enhancement in PEC performance of Ag-functionalized heterostructures can be attributed to efficient photon absorption and charge carrier generation/separation, originating from the SPR effects of Ag NPs and also the formation of the $CuWO_4/WO_3$ junction.

The long-term stability of the Ag-functionalized composite photonode was evaluated by chronoamperometry and cyclic voltammetry (CV), performed under constant illumination. In spite of a primary descent in photocurrent (about 15%), the Ag-functionalized composite exhibited a steady-state current density of 0.178 mA/cm^2 over 2 hour (Fig. 7b) and only insignificant changes during frequent cycling (10 cycles, Fig. S4). The observed photocurrent loss corresponds to the formation of the Helmholtz layer, e.g. the interaction between the electrolyte anions and the photoelectrode surface. Moreover, the formation of peroxo species on the WO_3 surface is also likely [33, 62]. The presented results obviously reveal that Ag functionalized-composite films show decent stability during continuous water oxidation. In spite of significant PEC enhancement in this work, a high charge transfer resistance is still limiting the PEC performance. It is expected that more effective charge carrier transport/separation can be achieved by the addition of electron transfer mediators such as 1D metals or carbonaceous nanostructures, which is currently under investigation.

4. Conclusions

In summary, Ag-functionalized $CuWO_4/WO_3$ heterostructured photoanodes were successfully prepared via sol-gel synthesis and electrophoretic deposition. The as-produced Ag-composite films exhibited a 3-4-fold higher photocurrent density compared to pristine semiconductors, which was attributed to improved absorption properties, lower charge transfer resistance, higher separation efficiency of photo-generated charge carriers, and reduced electron/hole recombination supported by the detailed analysis of the obtained PEC data. Finally, the metal/semiconductor composite exhibited sufficient photostability and appears to be competitive in PEC performance.

5. Conflicts of interest

There are no conflicts of interest to declare.

6. Acknowledgement

The authors would like to acknowledge Color & Polymer Research Center (CPRC) for supporting this project. Also, Fig. 1 (just pure composite plot) and Fig. 3 (just pure composite and WO_3 plots) reproduced from our previous work (Ref. 39) with permission from the Centre National de la Recherche Scientifique (CNRS) and the Royal Society of Chemistry.

7. References

[1] M. G. Walter, E. L. Warren, J. R. McKone, S. W. Boettcher, Q. Mi, E. A. Santori, N. S. Lewis, Chem. Rev. 2010, **110**, 6446-6473

[2] R. V. De Krol, M. Gratzel, Photoelectrochemical Hydrogen Production, Springer, New York, NY, 2012.

[3] S. Ardo, D.F. Rivas, M.A. Modestino, V.S. Greiving et al. Energy Environ. Sci. 2018, **11**, 2768-2783

[4] H. Sameie, A.A. Sabbagh Alvani, N. Naseri, S. Du, F. Rosei, Ceram. Int. 2018, **44**, 6607-6613

[5] M.G.C. Zoontjes, K. Han, M. Huijben, W.G. van der Wiel, G. Mul, Catal. Sci. Technol., 2016, **6**, 7793-7799

[6] H. Sameie, A.A. Sabbagh Alvani, N. Naseri, F. Rosei, G. Mul, B.T. Mei, J. Electrochem. Soc. 2018, **165**, H353-H359

[7] C. Marchal, M. Behr, F. Vigneron, V. Caps, V. Keller, New J. Chem., 2016, **40**, 4428-4435

[8] M. Gholami, M. Qorbani, O. Moradlou, N. Naseri, A. Z. Moshfegh, RSC Adv. 2014, **4**, 7838-7844

[9] J. Mahajan, P. Jeevanandam, New J. Chem., 2018, **42**, 2616-2626

[10] Y. Ling, G. Wang, D.A. Wheeler, J.Z. Zhang, Y. Li. Nano Lett. 2011, **11**, 2119-2125

[11] S. Kment, F. Riboni, S. Pausova, L. Wang, L. Wang, H. Han, Z. Hubicka, J. Krysa, P. Schmuki, R. Zboril, Chem. Soc. Rev. 2017, **46**, 3716-3769
[12] C. Das, P. Roy, M. Yang, P. Schmuki, Nanoscale. 2011, **3**, 3094-3096
[13] J.E. Yourey, K.J. Pyper, J.B. Kurtz, B.M. Bartlett, J. Phys. Chem. C. 2013, **117**, 8708-8718
[14] C.R. Lhermitte, B.M. Bartlett, Acc. Chem. Res. 2016, **49**, 1121-1129
[15] J.E. Yourey, B.M. Bartlett, J. Mater. Chem. 2011, **21**, 7651-7660.
[16] Z. Ma, O. Linnenberg, A. Rokicinska, P. Kustrowski, A. Slabon, J. Phys. Chem. C. 2018, **122**, 19281-19288
[17] Y. Gao, T.W. Hamann, Chem. Commun. 2017,**53**, 1285-1288
[18] M. Valenti, D. Dolat, G. Biskos, A. Schmidt-Ott, W. A. Smith, J. Phys. Chem. C. 2015, **119**, 2096-2104
[19] R.K. Selvan, A. Gedanken, Nanotechnology. 2009, **20**, 105602-105609
[20] X. Liu, F. Wang, Q. Wang, Phys. Chem. Chem. Phys. 2012, **14**, 7894-7911
[21] I.A. Castro, G. Byzinski, M. Dawson, C. Ribeiro, J. Photochem. Photobiol. A: Chem. 2017, **339**, 95-102.
[22] G.H. Go, P.S. Shinde, C.H. Doh, W.J. Lee, Mater. Des. 2016, **90**, 1005-1009
[23] S.S. Kalanur, I.H. Yu, H. Seo, Electrochim. Acta. 2017, **254**, 348-357
[24] N. Gaillard, Y. Chang, A. DeAngelis, S. Higgins, A. Braun, Int. J. Hydrog. Energy. 2013, **38**, 3166-3176
[25] H. Zhang, P. Yilmaz, J. O. Ansari, F. F. Khan, R. Binions, S. Krause and S. Dunn, J. Mater. Chem. A. 2015, **3**, 9638-9644
[26] F. Wang, C.D. Valentin, G. Pachionni, J. Phys. Chem. C. 2012, **116**, 8901-8909
[27] Y. Tang, N. Rong, F. Liu, M. Chu, H. Dong, Y. Zhang, P. Xiao, App. Surf. Sci. 2016, **361**, 133-140
[28] Y. Liu, Y. Yang, Q. Liu, Y. Li, J. Lin, W. Li, J. Li, Journal of Colloid and Interface Science. 2018, **512**, 86-95

[29] Y. Liu, B.R. Wygant, O. Mabayoje, J. Lin, K. Kawashima, J.H. Kim, W. Li, J. Li, C.B. Mullins, ACS Appl. Mater. Interfaces, 2018, **10**, 12639-12650

[30] K.C. Leonard, K.M. Nam, H.C. Lee, S.H. Kang, H.S. Park, A.J. Bard, J. Phys. Chem. C. 2013, **117**, 15901-15910
[31] J. Zhu, W. Li, J. Li, Y. Li, H. Hu, Y. Yang, Electrochim. Acta. 2013, **112**, 191-198
[32] D. Hu, P. Diao, D. Xu, Q. Wu, Nano Research. 2016, **9**, 1735-1751
[33] K.M. Nam, E. A. Cheon, W. J. Shin, A.J. Bard, Langmuir. 2015, **31**, 10897-10903
[34] S.K. Pilli, T.G. Deutsch, T.E. Furtak, L.D. Brown, J.A. Turner, A.M. Herring, Phys. Chem. Chem. Phys., 2013, **15**, 3273-3278
[35] J. Li, S.K. Cushing, F. Meng, T.R. Senty, A.D. Bristow, N. Wu, Nat. Photonics. 2015, **9**, 601-607
[36] A. Verma, A. Srivastav, S.A. Khan, V. R. Satsangi, R. Shrivastav, D. K. Avasthib, S. Dass, Phys. Chem. Chem. Phys. 2017, **19**, 15039-15049
[37] M. Davi, A. Drichel, M. Mann, T. Scholz, F. Schrader, A. Rokicinska, P. Kustrowski, R. Dronskowski, A. Slabon, J. Phys. Chem. C, 2017, **121**, 26265-26274
[38] Q. Zhang, D. T. Gangadharan, Y. Liu, Z. Xu, M. Chaker, D. Ma, J. Materiomics. 2017, **3**, 33-50
[39] R. Salimi, A.A. Sabbagh Alvani, N. Naseri, S.F. Du, D. Poelman, New J. Chem. 2018, **42**, 11109-11116
[40] K. Han, Y.C. Lin, C.M. Yang, R. Jong, G. Mul, B. Mei, ChemSusChem. 2017, **10**, 4510-4516
[41] A. L Patterson, Phys. Rev. 1939, **56**, 978-982
[42] R. Salimi, H. Sameie, A.A. Sabbagh Alvani, A.A. Sarabi, F. Moztarzadeh, M. Tahriri, Luminescence, **26**, 449-455
[43] S. Kandhasamy, A. Pandey, M. Minakshi, Electrochim. Acta. 2012, **60**, 170-176
[44] N. Soltani, E. Saion, M. Erfani, K. Rezaee et al, Int. J. Mol. Sci. 2012, **13**, 12412-12427

[45] C. Su, L. Liu, M. Zhang, Y. Zhang, C. Shao, CrystEngComm, 2012, **14**, 3989-3999
[46] R.K. Selvan, A. Gedanken, Nanotech. 2009, **20**, 105602-105609
[47] F. Liu, X. Chen, Q. Xia, L. Tian, X. Chen, RSC Adv. 2015, **5**, 77423-77428
[48] S. Dey, R.A Ricciardo, H.L. Cuthbert, P.M. Woodward, Inorg. Chem. 2014, **53**, 4394-4399.
[49] M. Valenti, M. P. Jonsson, G. Biskos, A. Schmidt-Ott, W. A. Smith, J. Mater. Chem. A, 2016, **4**, 17891-17912.
[50] R. Salimi, A.A. Sabbagh Alvani, N. Naseri, Nanomaterials: Application & Properties (NAP), 2017, IEEE 7th International Conference, Odessa, Ukraine
[51] D. Bohra, W.A. Smith, Phys. Chem. Chem. Phys. 2015, **17**, 9857-9866
[52] H. Chen, W. Leng, and Y. Xu, J. Phys. Chem. C. 2014, **118**, 9982-9989
[53] H. Dotan, K. Sivula, M. Gratzel, A. Rothschild, S.C. Warren, Energy Environ. Sci. 2011, **4**, 958-964
[54] W. Ye, F. Chen, F. Zhao, N. Han, Y. Li, ACS Appl. Mater. Interfaces. 2016, **8**, 9211-9217
[55] C. Wang, Z. Chen, H. Jin, C. Cao, J. Li, Z. Mi, J. Mater. Chem. A. 2014, **2**, 17820-17827
[56] W. Guo, Z. Duan, O. Mabayoje, W. D. Chemelewski, P. Xiao, G. Henkelman, Y. Zhang, C. B. Mullins, J. Electrochem. Soc. 2016, **163**, H970-H975
[57] L.C. Sim, K.H. Leong, S. Ibrahim, P. Saravanan, J. Mater. Chem. A. 2014, **2**, 5315-5322
[58] M.A. Butler, D.S. Ginley, J. Electrochem. Soc. 1978, **125**, 228-232
[59] F. Opoku, K.K. Govender, C.G. Catharina Elizabeth van Sittert, P.P. Govender, Phys. Chem. Chem. Phys. 2017, **19**, 28401-28413
[60] S.C. Warren, E. Thimsen, Energy Environ. Sci. 2012, **5**, 5133-5146

[61] B. K. Russell, J. G. Mantovani, V. E. Anderson, R. J. Warmack, T. L. Ferrell, Physical Review B, 1987, 35, 2151-2154
[62] J. C. Hill, K.S. Choi, J. Phys. Chem. C. 2012, **116**, 7612-7620